

Mapping clay minerals in an open-pit mine using hyperspectral imagery and automated feature extraction

Richard J. Murphy, Sven Schneider, Zachary Taylor & Juan Nieto
Australian Centre for Field Robotics, University of Sydney, Australia
richard.murphy@sydney.edu.au, +61 2 9114 0897

Abstract

The ability to map clay minerals on vertical geological surfaces is important from perspectives of stratigraphical mapping of geological units and safety. Clay minerals represent lines of stratigraphical weakness along which landslides can occur. To map clay minerals on complex geological surfaces we use a combination of hyperspectral and LiDAR data. These data are automatically registered to provide a map of the distribution of clay minerals and their abundances at different spatial scales.

Key words: Mine face, Hyperspectral imagery, LiDAR, Clay minerals, Absorption feature

1. Introduction

There have been many studies which have used hyperspectral imagery acquired from aircraft to map clays minerals (e.g. CRÓSTA et al., 1998; LAGACHERIE et al., 2008). Recently, there has been an increasing use of hyperspectral data acquired from field based platforms to map minerals as they are distributed on vertical outcrops of geology (KURZ et al., 2013; MURPHY et al., 2012). Various sensor and environmental effects make the calibration and analysis of these data more challenging (reviewed by KURZ et al., 2013). Methods used to extract information from hyperspectral data must be resistant to these effects.

The ability to recognise clays in outcrops of vertical geology is important for geological mapping and safety perspectives. Thin bands of shale are sometimes used as marker horizons to distinguish different geological units. Shales also represent lines of stratigraphical weakness along which landslides can occur (CORNFORTH, 2005; HANCOX, 2008; HUTCHINSON, 1961). Smectite group clays in particular can undergo large changes in volume through swelling which can cause localised instability and ground heave (GILL et al., 1996; GOETZ et al., 2001). Many techniques have been developed to classify minerals on the basis of their entire spectral curve in the Shortwave Infra-red (SWIR) where diagnostic absorption features of many minerals are located. However, several parameters of absorption features such as their wavelength position and depth can yield important information about aspects of the physical-chemical composition of minerals (BISHOP et al., 2008; MARTÍNEZ-ALONSO et al., 2002). We therefore use wavelength position as a way of

detecting and mapping diagnostic absorption features of clay minerals in the SWIR, at different spatial scales in an open-pit mine in Western Australia. To identify areas of thicker deposits of clay which have the potential to become unstable, we map the distribution of clays over the surface of one side of the entire mine pit (large-scale mapping). To identify thin shale bands as marker horizons to separate different geological units of similar spectral characteristics we use imagery of an individual mine face (small-scale mapping).

Automated feature extraction (AFE) was used to detect and parameterise absorption features. Hyperspectral imagery was automatically registered to LiDAR data of the same mine wall to generate 2.5D maps of absorption by clay minerals (TAYLOR et al., 2013).

2. Materials and methods

2.1 Hyperspectral imagery

Imagery was acquired from a single mine face and from a vertical section of the entire pit. Hyperspectral imagery (970 – 2500 nm) was acquired using an AISA HAWK hyperspectral imager (Specim, Finland). High temperatures (> 55° C) in the mine pit required that the sensor was enclosed in an insulated box and kept cool by passing cooled desiccated air over it. Calibration panels with different reflectance (80 % Teflon, 15 %, 30 %, 60 % and 99 % Spectralon) were placed in the field of view of the sensor.

Data were acquired under clear-sky conditions with the sun directly illuminating the mine wall.

2.2 LiDAR data

LiDAR scans of the mine pit were acquired to generate 3D point clouds of the scene. The laser scanner (Riegl LMS-Z620) was placed in close proximity to the hyperspectral sensor. A Trimble global position system (GPS) device was used to acquire GPS coordinates of the locations of the two sensors (i.e. the hyperspectral sensor and the laser scanner).

2.3 Calibration of hyperspectral imagery

Imagery was calibrated using a flat field calibration and, separately, the empirical line method (ROBERTS et al., 1986). The longest sensor-target distance was > 130m, thus path radiance may have had a small impact on spectra. Flat field calibration was done using 80 % Teflon calibration panel. Each pixel in each band was divided by the average of the pixels over the calibration panel for that band. The values were corrected to absolute reflectance using the reflectance factors of the calibration panel. Data were calibrated by the empirical line method using data from the 80 % Teflon and 15 % Spectralon panels.

2.4 Automated feature extraction (AFE)

The image was filtered using a polynomial smoothing filter with a width of 8-bands (SAVITZKY and GOLAY, 1964). Automated feature extraction was then used to identify the strongest (i.e. deepest) absorption feature between 2041 and 2380 nm and parameterise it in terms of its wavelength position, depth and width. Two thresholds were used. First, a feature is 'found' only if the hull-quotient value of the absorption feature minimum is less than 0.95. Preliminary work determined that this removed spurious absorption features from consideration. Second, a brightness threshold was set to remove from consideration all spectra which had an average brightness of less than 0.08. Spectra with a brightness of less than this threshold had a very low signal-to-noise ratio resulting in AFE 'finding' spurious absorption features. Wavelength position and depth for each pixel spectrum were described in separate grey-scale images.

2.5 Registration with LiDAR data

The hyperspectral imagery was automatically registered to the point cloud derived from the LiDAR using the method of TAYLOR et al. (2013). This method automatically determines the location and orientation of the camera relative to the LiDAR, as well as the cameras focal length. It achieves this by creating a camera model that projects the LiDAR data onto the hyperspectral image. The quality of the alignment between the

LiDAR and the hyperspectral image is evaluated by using a gradient orientation measure that compares the relative alignment of gradients. The unknown parameters of the camera model, in this case the location, orientation and focal length are found using particle swarm optimisation, which maximises this gradient measure.

3. Results

3.1 Reflectance calibration

Calibration to reflectance using the flat field approach and the empirical line method gave similar results. The curve shapes of spectra of selected minerals calibrated by each method were similar. Reflectance was, however, greater in spectra calibrated by the empirical line method were consistently greater than those calibrated by flat field correction.

3.2 Clay minerals - large -scale mapping

Separate images quantifying the wavelength position of the deepest absorption feature and its depth were generated using AFE. On the basis of wavelength position, six minerals were identified (figure 1). The illite-smectites were identified by their main absorption at 2202 nm in combination with a weak absorption at 2235 nm. Ferruginous (Fe) smectite was identified by absorptions at 2288 nm and 2220 nm related to both Fe and Al in octahedral sites.

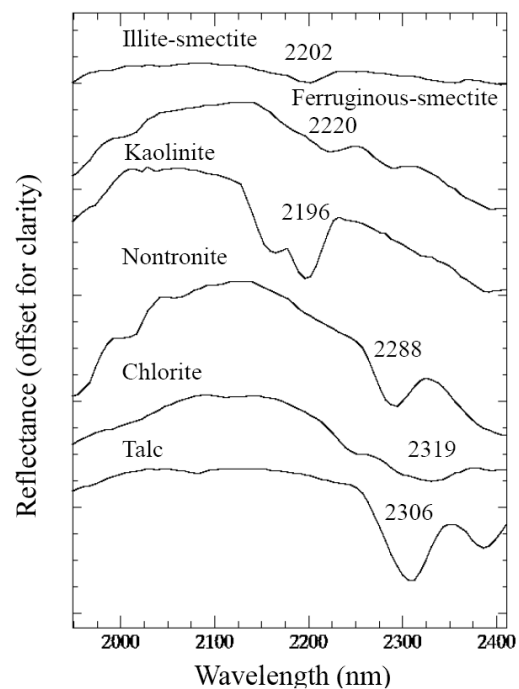


Fig. 1 : Single pixel spectra of minerals identified from the wavelength parameter image.

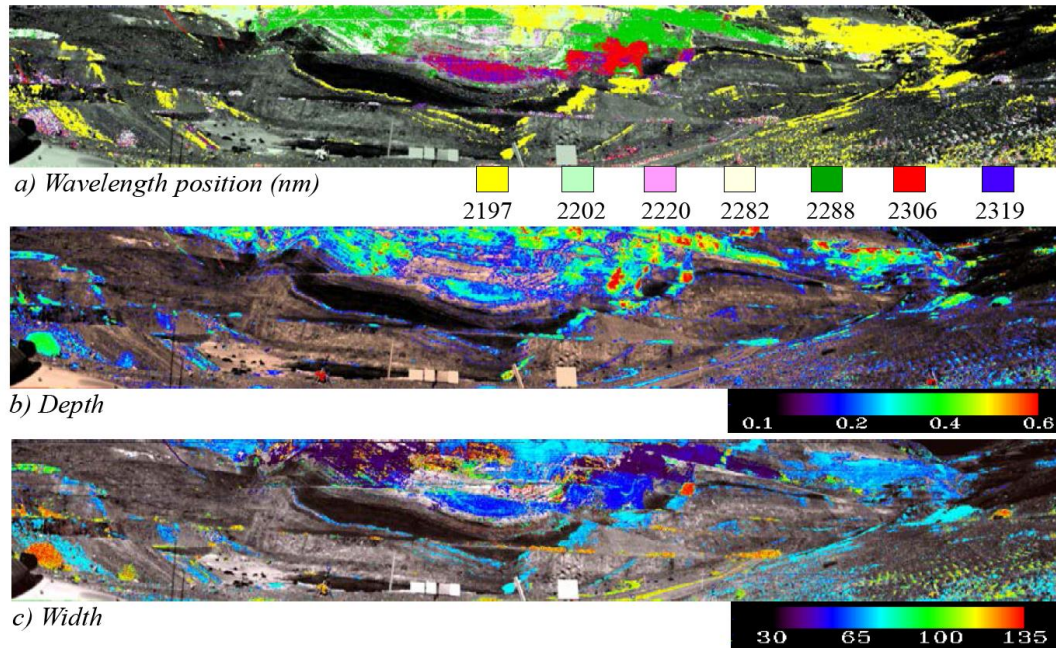


Fig. 2 : Absorption feature parameters wavelength position, depth and width for the large-scale mapping of the mine wall.

Nontronite was identified by a single feature at 2288 nm caused by Fe-OH and Kaolinite by the characteristic Al-OH absorption doublet at 2196 nm. Images of wavelength position, depth and width are shown in figure 2. The wavelength parameter image shows distinct, narrow layers are formed by several clay minerals including kaolinite but also much thicker (10s m) layers of nontronite were evident (figure 2a). Other minerals, e.g. chlorite, were present in discrete areas of the mine wall. Large spatial variations in the abundance of clay minerals, indicated by the depth parameter image, were found across the mine wall (figure 2b). The strongest absorptions were found for the minerals Talc, Nontronite and Kaolinite and the weakest for Illite-smectite and Fe-smectite. The width of absorption features varied from about 35 nm for illite-smectite and nontronite to 135 nm for chlorite (figure 2c).

3.3 Clay minerals – small-scale mapping

Clay layers were mapped in the field (figure 3a). These layers are used by geologists as marker horizons to separate different but spectrally indistinguishable geological units. Four distinct geological units were identified in the field and from X-ray diffraction analysis (figure 3a). These in-

cluded un-mineralised Banded Iron Formation (BIF; Unit 1), low-grade ore (Unit 2), and high-grade ore (Units 3 & 4). AFE identified the 3 clay layers that were mapped in the field (S1, S2 & S3). The wavelength parameter image shows that

the majority of absorption features were located at 2196 and 2202, associated with kaolinite and illite-smectite (Figure 3b). A few scattered pixels had absorption features at 2208, also indicative of illite-smectite. S1 was of different composition to S2 and S3. S1 was comprised of a mixture of pixels representing illite-smectite and kaolinite whereas 2 & 3 were composed mainly of kaolinite. Two narrower clay layers, not mapped in the field, were identified by AFE at the extreme left of the image. The clay absorptions mapped by AFE did not form contiguous linear features on the mine face. S1 & S2, in particular, had ‘gaps’ in clay absorption along their length. This was consistent with field observations. The gaps in the clay layers indicate that the abundance of clays in these areas was small and that the absorptions were too weak to be included in the depth threshold used by AFE to identify coherent absorption.

The depth parameter image showed that S1 & S2 had deeper absorptions than did S3 (figure 3c). Absorption feature width did not, however, provide any useful information.

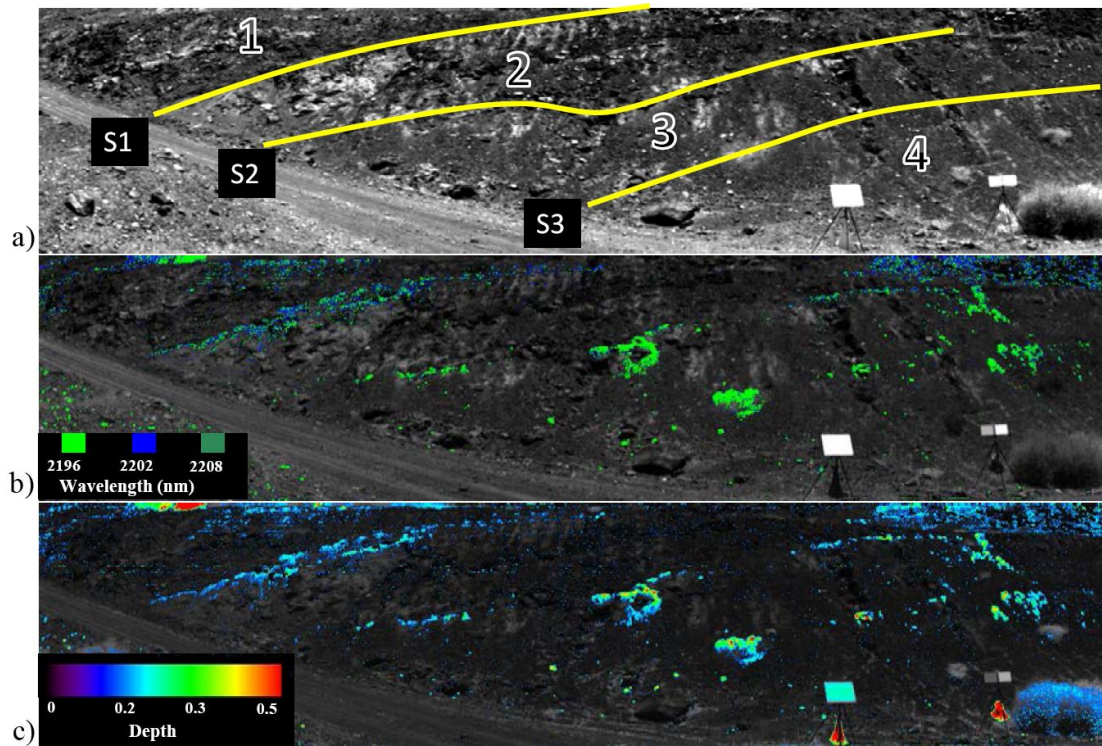


Fig. 3: Small-scale mapping of clay layers on a mine face: a) Greyscale image with superimposed clay layers mapped from field observations (S1, S2 & S3). These layers are used as marker horizons to distinguish geological units of different composition but with similar spectral characteristics (Units 1, 2, 3 & 4); b) Wavelength parameter image; c) depth parameter image.

3.4 Maps of minerals in 2.5 D space

Using the parameters from the projection of the hyperspectral image from the large-scale mapping onto the LiDAR data, 2.5D maps of mineral distribution were created from the wavelength parameter image (figure 4). From the 2D images (figure 2) it is extremely difficult to determine perspective in relation to the mine pit. The 2.5 D maps clearly show that the greatest variation in the types of clay minerals occurs towards the base of the mine pit in a region of complex synclinal folding.

4. Discussion and conclusions

AFE has been used in this study to identify and map clay absorptions from hyperspectral imagery at small and large scales. The advantage of AFE

is that no prior knowledge is required and it can be used without a spectral library. AFE success-

fully identified clay layers on a mine wall, allowing separation of geological units which would have otherwise been indistinguishable using optical means. At the larger spatial scale clay minerals were mapped for the entire mine pit. This has significant potential for predicting which areas of the mine pit are susceptible to failure. The ability to combine, automatically, products derived from hyperspectral imagery with LiDAR data greatly improves the scope of applications for its use. For example, combining information on clay minerals with information on aspects of geometry (e.g. slope, aspect) enables pertinent, spatially referenced information to be incorporated into models of slope stability. Work is currently underway to determine the best ways in which information from the various absorption feature parameters can be combined into meaningful thematic maps.

The development of field-based hyperspectral systems has opened up new possibilities for its use in the identification and mapping of minerals on natural and artificial vertical geological surfaces.

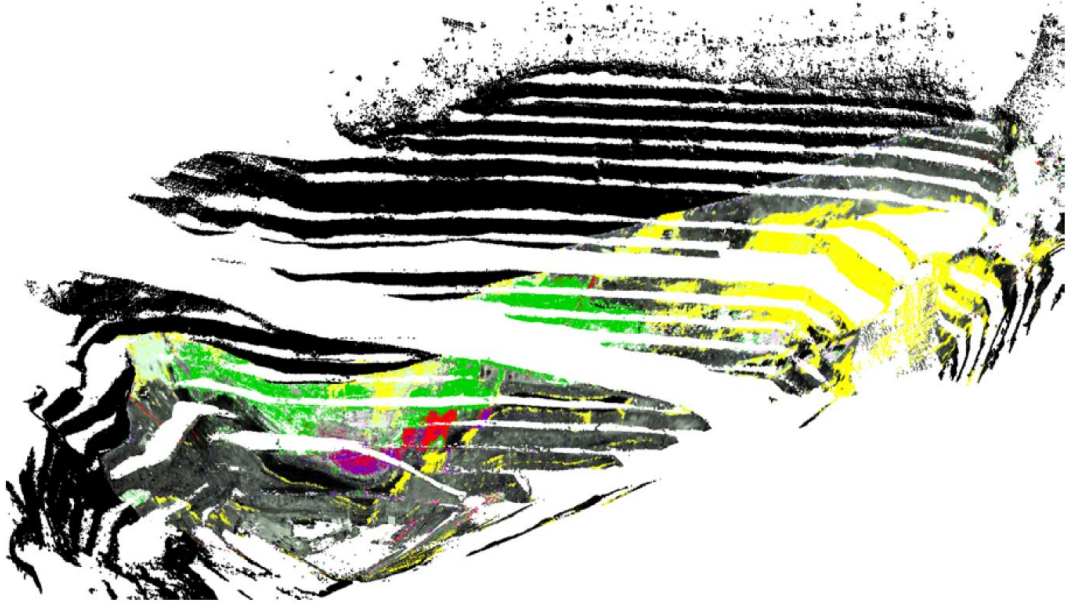


Fig. 4: 2.5 D map of clay minerals for the large-scale mapping: wavelength position registered to the LiDAR data. Locations mapped by LiDAR, but not by the hyperspectral sensor, are shown as black.

Acknowledgements: This work has been funded by the Australian Centre for Field Robotics and the Rio Tinto Centre for mine Automation. We are grateful to Dr Geoff Carter for his help with the logistics of data collection and access to the mine.

References

- BISHOP, J.L., LANE, M.D., DYAR, M.D. & BROWN, A.J. (2008): *Reflectance and emission spectroscopy study of four groups of phyllosilicates: smectites, kaolinite-serpentines, chlorites and micas*: Clay minerals, v. 43, 35-54.
- CORNFORTH, D.H. (2005): *Landslides in Practice - Investigation, Analysis, and Remedial/Preventative Options in Soils*, John Wiley & Sons.
- CRÓSTA, A.P., SABINE, C. & TARANIK, J.V. (1998): *Hydrothermal Alteration Mapping at Bodie, California, Using AVIRIS Hyperspectral Data*: Remote Sensing of Environment, v. 65, 309-319.
- GILL, J.D., WEST, M.W., NOE, D.C., OLSEN, H.W. & MCCARTY, D.K. (1996): *Geologic control of severe expansive clay damage to a subdivision in the Pierre Shale, Southwest Denver Metropolitan area, Colorado*: Clays and Clay Minerals, v. 44, 530-539.
- GOETZ, A.F.H., CHABRILLAT, S. & LU, Z. (2001): *Field reflectance spectrometry for detection of swelling clays at construction sites*: Field Analytical Chemistry & Technology, v. 5, 143-155.
- HANCOX, G.T. (2008): *The 1979 Abbotsford Landslide, Dunedin, New Zealand: a retrospective look at its nature and causes*: Landslides, v. 5, 177-188.
- HUTCHINSON, J.N. (1961): *A Landslide on a Thin Layer of Quick Clay at Furre, Central Norway*: Geotechnique, v. 11, 69-94.
- KURZ, T.H., BUCKLEY, S.J. & HOWELL, J.A. (2013): *Close-range hyperspectral imaging for geological field studies: Workflow and methods*: International Journal of Remote Sensing, v. 34, 1798-1822.
- LAGACHERIE, P., BARET, F., FERET, J.-B., MADEIRA NETTO, J. & ROBBEZ-MASSON, J.M. (2008): *Estimation of soil clay and calcium carbonate using laboratory, field and airborne hyperspectral measurements*: Remote Sensing of Environment, v. 112, 825-835.
- MARTÍNEZ-ALONSO, S., RUSTAD, J.R. & GOETZ, A.F.H. (2002): *Ab initio quantum mechanical modeling of infrared vibrational frequencies of the OH group in dioctahedral phyllosilicates. Part II: Main physical factors governing the OH vibrations*: American Mineralogist, v. 87, 1224-1234.
- MURPHY, R.J., MONTEIRO, S.T. & SCHNEIDER, S. (2012): *Evaluating Classification Techniques for Mapping Vertical Geology Using Field-Based Hyperspectral Sensors*: IEEE Transactions on Geoscience and Remote Sensing, v. 50, 3066-3080.
- ROBERTS, D.A., YAMAGUCHI, Y. & LYON, R.J.P. (1986): *Comparison of various techniques for calibration of AIS data*, in VANE, G. & GOETZ, A.F.H., eds., Second Airborne Imaging Spectrometer Data Analysis Workshop, Volume JPL Publication 86-35: Pasadena, California, NASA Jet Propulsion Laboratory, p. 21-30.

SAVITZKY, A. & GOLAY, M.J.E. (1964): *Smoothing and differentiation of data by simplified least squares procedures*: Analytical Chemistry, v. 36, 1627-1639.

TAYLOR, Z., NIETO, J. & JOHNSON, D. (2013): Automatic calibration of multi-modal sensor systems using a gradient orientation measure, IEEE International Conference on Intelligent Robots and Systems.